Material Behaviour

Molecular orientation dependent dynamic viscoelasticity in uni-axially drawn polycarbonate

Fei Luo[a,b], Xianhu Liu[a,*], Chenguang Yan[c], Hu Liu[a,e], Mengyao Dong[a,e], Xianmin Mai[d], Changyu Shen[a,b], Chuntai Liu[a,**], Jiaoxia Zhang[e,f], Ning Wang[g], Zhanhu Guo[e,***]

[a] National Engineering Research Center for Advanced Polymer Processing Technology, Zhengzhou University, Zhengzhou, Henan, 450002, China
[b] College of Materials Science and Engineering, Zhengzhou University, Zhengzhou, Henan, 450001, China
[c] School of Mechanical and Electrical Engineering, Zhoukou Normal University, Zhoukou, Henan, 466001 China
[d] School of Urban Planning and Architecture, Southwest Minzu University, Chengdu 610041, China
[e] Integrated Composites Laboratory (ICL), Department of Chemical & Biomolecular Engineering, University of Tennessee, Knoxville, TN, 37996, USA
[f] School of Material Science and Engineering, Jiangsu University of Science and Technology, Zhenjiang, Jiangsu, 212003, China
[g] State Key Laboratory of Marine Resource Utilization in South China Sea, Hainan University, Haikou, China

ARTICLE INFO

ABSTRACT

Molecular orientation and dynamic modulus of the high and low temperature drawn polycarbonate splines were investigated using wide-angle X-ray diffraction (WAXD) and dynamic mechanical analysis (DMA). For high-temperature stretched splines, the storage modulus in the glassy state and the loss modulus in the rubbery state increased with increasing the orientation. No obvious regularity was observed for the low-temperature stretched ones. These behaviors could be interpreted by a relation between relaxation modulus and average orientation angle, which was derived from the elastic dumbbell model and wormlike chain model. Through associating the molecular orientation defined by Herman's factor with the storage modulus at the end of the glassy state plateau and the loss modulus at the tanδ peak respectively, the relationship between orientation and dynamic viscoelasticity of polycarbonate was built as well.

1. Introduction

One of the main microscopic origin of the viscoelastic behavior of polymer is molecular orientation. Therefore, understanding the relationship between performances and oriented structure is very significant for revealing the mechanism of orientation [1–6]. So far, many viscoelastic theories and models have been developed for molecular motion, such as bead-rod chain model [7,8], bead-spring model [9], blob model [10], reputation model [11–13] and network model [14]. But most of molecular theories are very complicated and often used in solutions, melts and rubber-like states, the experimental proof of the molecular theories in glass-like state was rarely operated. Meanwhile, the existent characterization methods of molecular orientation, such as optical birefringence method [15,16], acoustic method [17], polarized laser Raman spectrometry [18–20], fourier transform infrared spectrometry [21], wide-angle X-ray diffraction (WAXD) [22,23] and contact angle method [24] can't easily determine the global orientation without being coupled with other appliances. However, the average

orientation and related viscoelasticity are more important than the local oriented state and property for the usability.

Polycarbonate (PC) has become increasingly interesting since its introduction in the 1960s because it can be used in electronics, automobile, medical instruments and aerospace, but the easy degradation and cracking of its products challenge its wide applications [25,26]. The viscoelastic phenomena caused by molecular motions of polymer chains play an important role in formability and stability [27–29]. Therefore, in order to decrease the failure of PC products, it is important to understand the relationship between orientation and viscoelasticity.

In order to characterize the global orientation and viscoelasticity of PC, in this paper the dynamic mechanical analysis (DMA) is used, which can probe the thermomechanical properties of materials and afford a simple approach to determine the microstructural relaxation in a global situation [29–33]. Moreover, it can determine the viscoelasticity of materials in a wide temperature range from the glassy state to the rubbery state. Furthermore, the oriented structure in the polymers will

not change dramatically below the glass transition temperature (T_g) and can be associated with the viscoelasticity easily in DMA. The average orientation, loss and storage modulus of the uni-axially stretched PC samples were studied by WAXD and DMA respectively. The PC samples were stretched at two temperatures at the same tensile rates. Through comparing the differences of loss and storage modulus among different oriented states, we expect to have a better understanding of the relationship between orientation and viscoelasticity. A relation between relaxation modulus and average orientation angle with Deborah number was deduced from the Elastic Dumbbell model and Wormlike chain model [34]. The experimental results and theories were combined together to build the pseudo dynamic relationship between orientation and viscoelasticity through the static images.

2. Theory

2.1. Orientation relaxation

A classical molecular statistical model, Elastic Dumbbell model, was used to calculate the molecular orientation [34]:

$$\frac{D}{Dt}\underline{A} - \underline{\nabla v^T}\cdot\underline{A} - \underline{A}\cdot\underline{\nabla v} = -\frac{1}{\lambda}\underline{A} + \underline{\nabla v} + \underline{\nabla v^T} \tag{1}$$

$$\underline{A} = 3\frac{<\underline{R}\ \underline{R}> - <\underline{R}\ \underline{R}>_0}{<R_0^2>} \tag{2}$$

where $\underline{A}$ is the deformation tensor of spring in the Elastic Dumbbell and represents a deviation of the chain with respect to the undisturbed conformation. The maximum eigenvalue of $\underline{A}$ can serve as the index to evaluate the orientation. The conformation tensor $<\underline{R}\ \underline{R}>$ equals to $<\underline{R}\ \underline{R}>_0$. $\underline{\nabla v}$ is the velocity gradient tensor. Molecular orientation generally contains two opposite processes, i.e., elongation and retraction of molecular chains [35]. It is easier to determine the orientation relaxation separately, the related molecular relaxation equation can be deduced from Eq. (1) by assuming that all the velocity gradient terms are zero:

$$\underline{A} = \underline{A}_0\exp\left(-\frac{t}{\lambda}\right) \tag{3}$$

where t is time and λ is relaxation time, $\underline{A}_0$ represents the initial orientation. Eq. (3) is similar to the strain recovery equation ($\underline{\varepsilon} = \underline{\varepsilon}_0\exp\left(-\frac{t}{\lambda}\right)$) deduced from the Voigt model and the stress relaxation equation ($\underline{\sigma} = \underline{\sigma}_0\exp\left(-\frac{t}{\lambda}\right)$) from the Maxwell model [36,37]. Considering the theoretical linear relationship between the orientation and flow induced stress [38], it is verified that Eq. (3) could be used to present molecular relaxation.

2.2. Orientation and modulus

The wormlike chain model proposed by Porod and Kratky succeeded in describing the semi rigid macromolecules [39–41]. The definition of persistence length, projected length, bond angle and length are very instructive. If the persistence length and projected length are regarded as molecular orientation in a specific direction, the bond is replaced by segment and the bond angle is transformed into the orientation angle. Suppose the macromolecule is a freely jointed chain, including a great number of segments and the length of each segment is l. The average angle between two adjacent segments is ϕ. If the first segment is parallel with the orientation direction, the mean projection of the whole molecular chain along the orientation can be obtained, as is shown in following equation.

$$< z> = l + l\cos\phi + l\cos^2\phi + \cdots + l\cos^{n-1}\phi = \frac{1 - \cos^n\phi}{1 - \cos\phi}l \tag{4}$$

For an infinite long chain, $n\to\infty$, $\cos^n\phi\to0$, Eq. (4) can be further converted into Eq. (5):

$$a = \lim_{n\to\infty}\ < z> = \frac{l}{1 - \cos\phi} \tag{5}$$

a is the persistence length, represents the trend of the whole molecular chain arranged in a certain direction. The cosine of average orientation angle is:

$$<\cos\phi'> \approx \frac{a}{nl} \approx \frac{1}{n(1 - \cos\phi)} \tag{6}$$

where $<\cos\phi'>$ is the cosine of average orientation angle. When the molecular orientation reaches the maximum, $<\cos\phi'>\to1$, $\cos\phi\to1$. The $<\cos\phi'>$ can be approximately replaced with $<\cos\phi>$, which has the similar meaning as the parameter defined in the Hermans' factor. If the segment is further divided and ϕ is reduced infinitely, i. e., $\phi\to0$, $\cos\phi\to1$, the macromolecule would change from a polygonal line with sharp edges to a wormlike line. Based on the Taylor series expansion, exp (-l/a) can be transformed into a cosine function (Eq. (7)), when the higher order terms are ignored.

$$e^{-\left(\frac{l}{a}\right)} = e^{-(1-\cos\phi)} \approx \cos\phi \tag{7}$$

Molecular segment is assumed as the smallest active structural unit to be considered, the related time t can be defined as the observation time. The persistence length a represents the trend of the whole molecular chain arranged in a certain direction, the related time is relaxation time λ. According to scaling theory and affine deformation assumption [42], the velocity gradients in multiscale are equal. Through assuming the velocity gradient was zero, the orientation calculation equation (1) was converted into a relaxation form (Eq. (3)). Furthermore, the deformation rate of macromolecule is similar to that of microstructure unit based on that assumption [9,34,43]. The relationship between two types of velocity is shown in Eq. (8).

$$\frac{l}{t} \approx \frac{a}{\lambda} \tag{8}$$

The modulus relaxation ($E(T)$) can be transformed into a cosine function as shown in Eq. (9):

$$E(T) = E_{min} + \Delta E\cdot exp\left(-\frac{1}{De}\right) \approx E_{min} + \Delta E\cdot < \cos\phi> \tag{9}$$

with De being expressed as Equation (10) [44]:

$$De = \frac{\lambda}{t} \tag{10}$$

where E_{min} is the elastic modulus of the un-oriented sample, $E_{min} + \Delta E$ represents the modulus of stretched sample at the beginning of relaxation. De is the Deborah number, which can be used to characterize the flow of amorphous polymer. As the De increases, the material is close to elasticity; on the contrary, it is close to viscosity. Furthermore, the De number is increased with increasing a if the assumed Eq. (8) is held. a is the tendency of molecular chain to keep the orientation. Eq. (9) suggests that the orientation and elastic modulus have similar time dependence during relaxation.

3. Experimental

3.1. Material and sample preparation

The optical grade polycarbonate (PC, 110, Chi-Mei Co.) with a density of $1.2\,g\,cm^{-3}$ and a melt flow rate (MFR) of 10 g/10min (300 °C, 1.2 kg, ASTM D1238) was used because it displayed molecular orientation when drawn in the solid state. The initial standard dumbbell-shaped tension sample with a thickness of 4 mm was produced by a Demag precision injection molding machine (Demag Plastics Group, Germany). The melt temperature and mold temperature were 295 and 80 °C, respectively. The packing pressure was 65 MPa. Then the sample was uni-axially drawn on a Shimadzu tensile machine (AG-X plus),
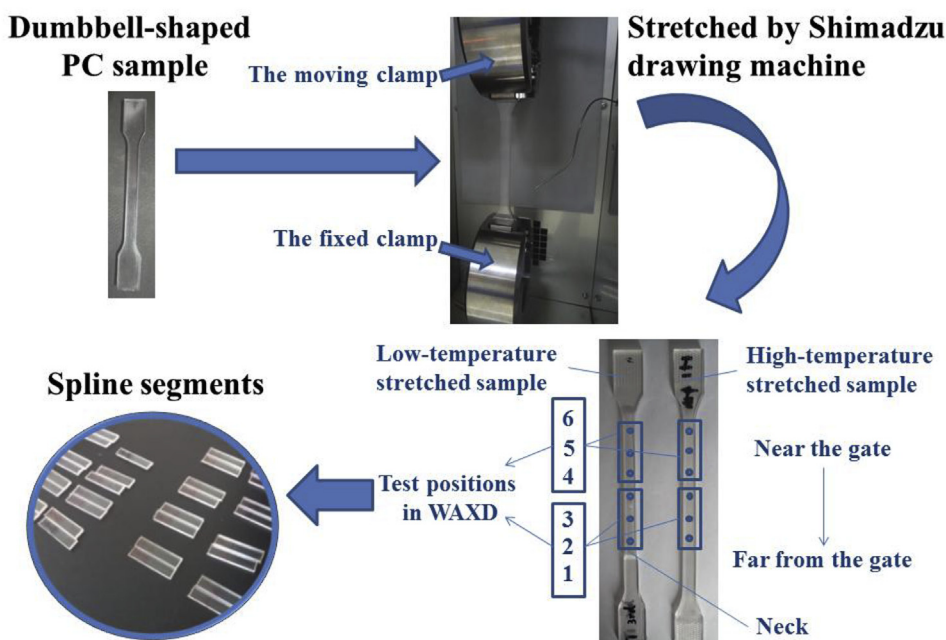
Fig. 1. Sample preparation. (The number of "1, 2, 3, 4, 5 and 6" represent the test locations of WAXD from far to near the gate.)

equipped with a temperature-controlled oven. The drawing temperatures were respectively chosen at low-temperature (30 °C) and high-temperature (130 °C). Prior to stretching, the samples were held for 5 min at the chosen temperature, in order to insure thermal stabilization. Four drawn speeds of 5, 10, 20 and 40 mm/min were used, and the stretching stroke was 50 mm. After drawing, the neck parts of the samples were further cut into segments with 35 mm length for WAXD and DMA experiments. The whole process of sample forming was shown in Fig. 1.

3.2. WAXD

WAXD was carried out on a Bruker Nanostar system. The Cu K_α radiation source (λ = 0.154 nm) was selected with a point focusing monochromator. The distance between the sample and the detector was 8.5 cm and the generator settings were 45 kV and 0.67 mA. The WAXD patterns were recorded using a Hi-STAR two-dimensional area detector. The Hermans' factor (Eq. (11)) coupled with Eq. (12) were used to illustrate the orientation quantitatively [19,45].

$$f = \frac{3 < cos^2\phi > - 1}{2} \qquad (11)$$

$$<cos^2\phi> = \frac{\int_0^{\pi/2} I(\phi)cos^2\phi sin\phi d\phi}{\int_0^{\pi/2} I(\phi)sin\phi d\phi} \qquad (12)$$

where f is the Hermans' factor, $I(\phi)$ is the scattering intensity at ϕ, $<cos^2\phi>$ is the square of average orientation parameter defined by Hermans' factor. Radial intensity profiles were obtained by azimuthal integration of the 2D patterns from 0° to 360°. The orientation of amorphous polymer was further calculated by Eqs. (11) and (12) over the 2θ range from 0° to 180° using the nonlinear curve fitting. The average orientations of samples were calculated and listed in Table 1.

3.3. DMA

A mechanical analyzer (Q800, TA Instruments, USA) was used in dynamic viscoelasticity testing and operated at a fixed frequency of 1 Hz in single cantilever mode. The temperature investigated was maintained at 40 °C for 3 min at the initial stage, then, heated up to

160 °C with a heating rate of 3 °C/min. The resultant storage loss, loss modulus and tanδ were recorded in the process.

4. Results and discussions

4.1. Orientation

Fig. 2 shows a 2D-WAXD pattern of the un-stretched PC sample. The isotropic reflection circle indicates a low orientation degree of the injection-molded PC sample [46–49]. Fig. 3 shows the distinct arcs of the stretched PC samples, rather than isotropic circles in Fig. 2. For samples under the high-temperature drawing, the diffraction arcs become more concentrated with increasing the distance in the equatorial direction from the gate to the test location (for example, from 6 to 1) as shown in Fig. 3a. But for the low-temperature drawing samples, the position dependence of 2D-WAXD patterns is not obvious. The equatorial arcs of low-temperature stretched samples are more concentrated than those of high-temperature stretched samples, which represent a greater orientation for the former than the latter ones. Table 1 illustrates the average orientation difference numerically between high and low temperature. Since higher temperature provides more free volume for molecular orientation and relaxation simultaneously, the absolute elongation of molecules is minimized by chain slip [50]. This regularity of position-dependent orientation at high temperature is also clearly shown in Table 1, which shows that all the average Hermans' factors near the gate are smaller than those far from the gate at high temperature. According to the seven parameters WLF equation, free volume is partly dependent on pressure. It is conceivable that the pressure drop along the flow direction in injection molding creates different free volume in the sample. The free volume affords necessary space for molecules moving. The larger free volume in the region far from the gate than near the gate is responsible for the position dependence of orientation. Whereas, the WAXD patterns and Hermans' factor at low temperature show irregularity. The possible reason is as follows: the molecular chains are considered to be frozen at far below the glass transition temperature, unless the micro-structure barrier was destroyed by an external loading. But the destruction at low temperature also results in a discontinuity of macro- and micro-structure. The molecules can be stretched more easily near the discontinued area, due to

Table 1
The Hermans' factor of the stretched PC samples.

Test Locations		High-temperature stretched samples				Low-temperature stretched samples			
		5[a]	10	20	40	5	10	20	40
Far from the gate	1	0.078	0.075	0.066	0.079	0.089	0.094	0.090	0.094
	2	0.075	0.066	0.070	0.070	0.090	0.088	0.091	0.093
	3	0.071	0.068	0.060	0.058	0.086	0.078	0.080	0.092
Average		0.075	0.070	0.066	0.069	0.088	0.087	0.087	0.093
Near the gate	4	0.070	0.054	0.050	0.053	0.091	0.090	0.095	0.099
	5	0.047	0.055	0.034	0.058	0.084	0.092	0.089	0.095
	6	0.053	0.046	0.038	0.045	0.086	0.090	0.088	0.091
Average		0.057	0.052	0.041	0.052	0.087	0.091	0.091	0.095

[a] The 5, 10, 20 and 40 represent the tensile rates of 5 mm/s, 10 mm/s, 20 mm/s and 40 mm/s, respectively.
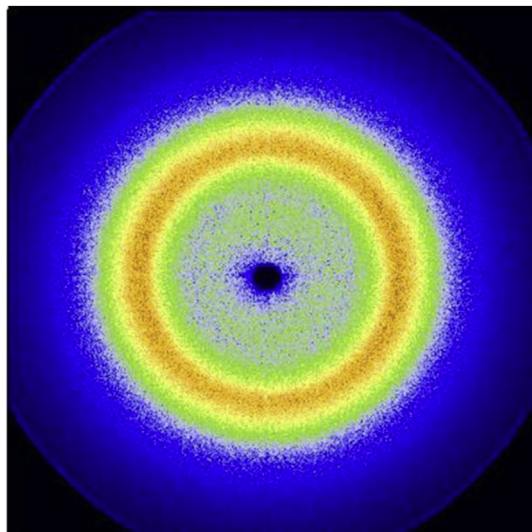

Fig. 2. WAXD patterns of un-stretched injection molded PC sample.

the extra volume causes local extension ratio increases faster than the continuum [51–53]. This type of fracture and discontinuity of structure is much smaller and more evenly distributed at high temperature. Table 1 also reveals the random change of Hermans' factor among different tensile rates no matter at high or low temperature since the final orientation degree is more likely controlled by the tensile stroke rather than tensile rate.

4.2. Orientation and elasticity

Although the viscoelasticity is considered dependent on both the orientation and free volume according to our previous research [2], the effects of free volume on viscoelasticity can be ignored in this experiment due to the same injection molding conditions, temperature and stroke of drawing. The oriented structure can be regarded as the most important single factor of the viscoelasticity. Fig. 4 shows the storage modulus plateau in the glassy state of different stretched PC samples. Compared with the high-temperature stretched sample, there is an unusual valley in the modulus plateau of low-temperature stretched sample. The v-shaped valley in the storage modulus curve can also be interpreted by the existence of fracture and discontinuity. The ramp down of the curve at the beginning of temperature rising reflects the decrease of the energy elasticity and the expansion of motion scale. The generated microstructural fractures can absorb energy and diminish the stress. The combined effects of temperature and fractures accelerate the decrease of storage modulus in the plateau through decreasing the stress, Fig. 4 (b). The following ramp-up part of the storage modulus curve, Fig. 4 (b), implies the possible fracture repair. At temperature close to the T_g, the polymer chains start to reshape to form the rubbery

network. Combined with Table 1, different heights of plateaus in Fig. 4 reflect different orientation-induced elasticity. In order to find the specific relationship between oriented state and elasticity, the storage modulus at the end of the plateau versus orientation calculated by WAXD is further plotted in Fig. 5. Fig. 5 (a) shows that the E' increases with increasing the orientation exponentially, i. e. the sample with a greater orientation has a larger storage modulus for high-temperature stretched samples. Nevertheless, the storage modulus of the low-temperature stretched samples is not closely associated with the orientation in Fig. 4 (b) and Fig. 5 (b). Fig. 1 shows the obvious necking phenomena in the low-temperature stretched samples, and Table 1 shows the uneven orientation of them at different test locations. Accordingly, the irregularity of modulus in the low-temperature stretched samples is caused by the molecular fragmentation, macroscopic crack, non-uniform macro-deformation and molecular orientation during drawing. Compared with the irregular results in Fig. 4 (b) and 5 (b), it is much easier to understand that the storage modulus is related to the orientation in Fig. 4 (a) and 5 (a).

The dynamic storage modulus E' at low frequency is approximately equal to the Young's modulus (E) in the steady-state. If replace E with E', the following Eq. (13) is obtained from Eq. (9):

$$E'(T) = E'_{min} + \Delta E' \cdot exp\left(-\frac{1}{De}\right) \tag{13}$$

For uni-axial orientation relaxation, the orientation tensor $\underline{A}$ can be replaced by the maximum eigenvalue α [34]. Eq. (3) can be transformed into Eq. (14):

$$\frac{\alpha(t)}{\alpha_0} = \frac{f(t)}{f'_0} = exp\left(-\frac{t}{\lambda}\right) \tag{14}$$

f'_0 and $f(t)$ represent the initial orientation and the time dependent orientation. Furthermore, $exp(-t/\lambda) \rightarrow 1 - t/\lambda$ because of $f(t)/f_0 \rightarrow 1$ in the early stage of the relaxation. The relationship between Hermans' factor and the storage modulus is obtained from Eq. (13):

$$E'(f) = E'_{min} + \Delta E' \cdot exp\left(-\frac{f}{f_0}\right) \tag{15}$$

The curve of Eq. (15) with proper parameters is shown in Fig. 5 (a), which is consistent with the change trend of the experiments. When $f \rightarrow f_0$, $De \rightarrow \infty$ according to Eqs. (10) and (14), i.e., a relatively greater orientation in the polymer corresponds to a larger De number and higher elasticity. This result indicates that the molecular chain becomes more rigid during the orientation. One explanation is that the free degree of the molecular segmental motion is minimized by stretching, and the orderly molecular alignment squeezed the free volume [54,55]. The motion became more difficult in segment-scale. Because the force-stretched chains can hardly be further stretched, molecular orientation leads to a smaller deformation of glassy polymer than the un-oriented polymer under a same external force, until the necking occurs [56].
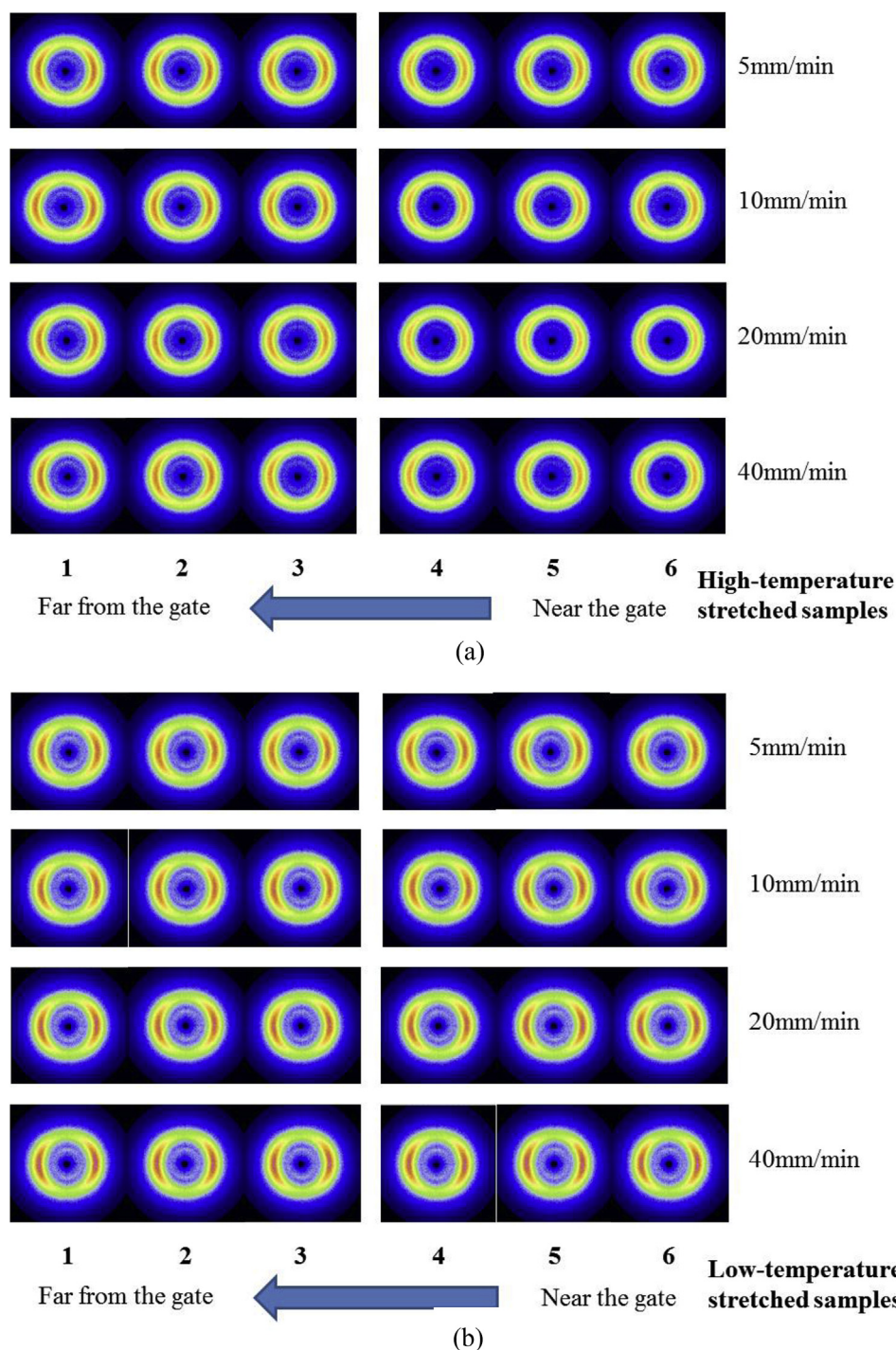
Fig. 3. WAXD patterns of PC specimens drawn at 130 °C (a) and 30 °C (b). (The drawing direction is vertical. The bottom number "1, 2, 3, 4, 5 and 6" have the same meaning as the number in Fig. 1.)

4.3. Orientation and viscosity

Fig. 6 shows the typical temperature-dependent curve of the loss modulus and tanδ. The relationship between viscosity and orientation is studied in the rubbery state, because the viscosity is unnoticeable in the glassy state and the oriented structure will be destroyed in the viscous flow state. A reference point corresponding to the peak of the tanδ is also marked in Fig. 6. The tanδ is defined as E''/E', which reflects the ratio of viscosity to elasticity. The maximum of the tanδ is commonly regarded as the T_g, and close to the T_g determined by DSC for PC. Therefore, the reference inflection point is considered as the upper

temperature limit of the segmental relaxation. As another significant signal of molecular motion, the loss modulus at the reference point can be approximately related to the orientation in the glassy state.

Fig. 7 shows that the loss modulus versus the orientation of the high-temperature stretched samples has a similar change trend to the storage modulus versus the orientation in Fig. 5 (a). The loss modulus increases with increasing the average orientation exponentially. But the dependence of loss modulus on the orientation in low-temperature samples is irregular. For the low-temperature samples, the cause for the irregularity of the loss modulus versus orientation is the same reason as that of the storage modulus versus orientation. For the high-
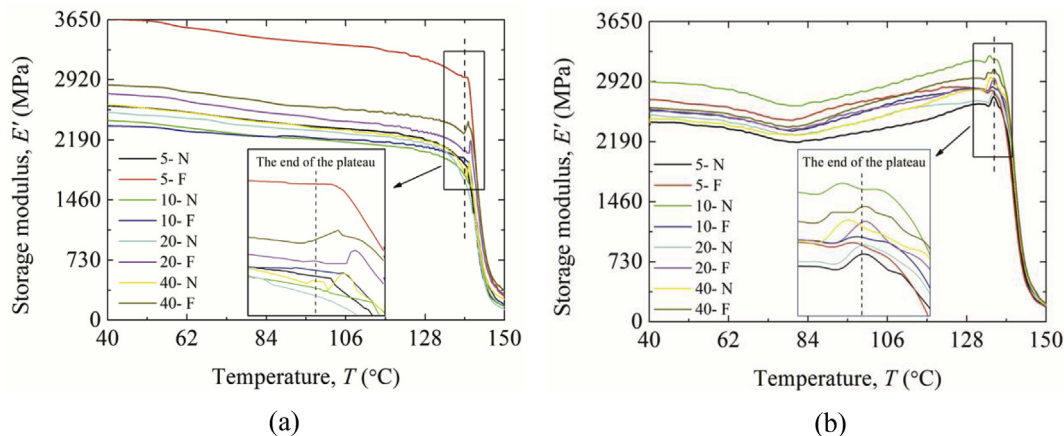
Fig. 4. Storage modulus of stretched PC samples at the end of the plateau phase. ((a) and (b) represent the high-temperature and low temperature conditions, respectively. F and N in legend represent samples far from the gate and near the gate, the DMA results of which correspond with the average molecular orientation calculated by WAXD in test locations "1, 2, 3" and "4, 5, 6" respectively.).
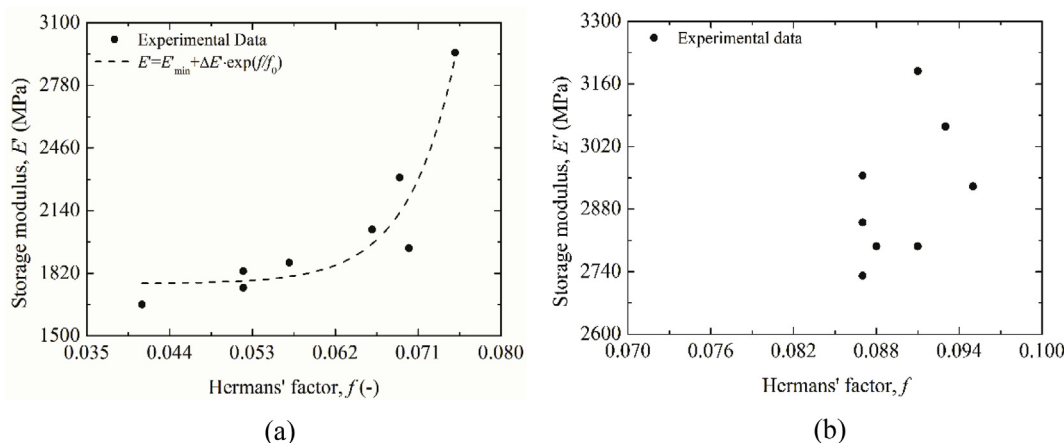

Fig. 5. The storage modulus versus Hermans' orientation factor of stretched samples. ((a) and (b) represent the high-temperature and low temperature conditions, respectively.).
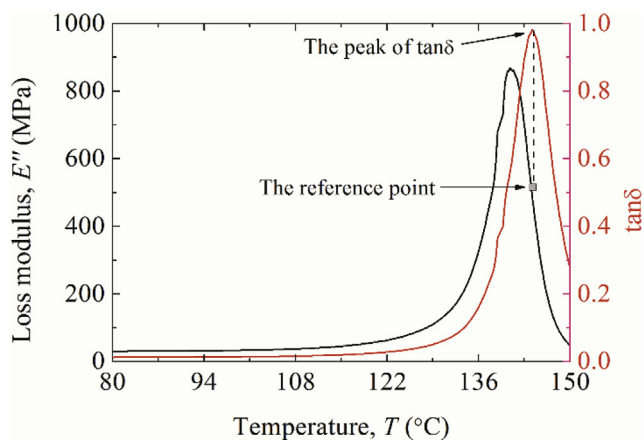

Fig. 6. The exemplary temperature dependent curves of loss modulus and tanδ in DMA.

temperature stretched samples, the increased viscosity is attributed to the increased orientation, which is perpendicular to the alternating loading direction in the single cantilever beam mode of DMA. The anisotropic viscosity of polymer has been shown to be greatly affected by orientation. Just as the assumptions in Reptation model suggested by de Gennes that a worm in a tube can only crawl along the tube, the

hindrance for molecular motion in the oriented system has a direction dependence. The *De* in Eq. (10) can also be used to explain the vertical directional viscosity decrease with orientation. The viscosity of polymer along the orientation decreases with increasing the *De*. Besides that, the molecules can be arranged more compact in the oriented state than in the random state, which further promotes the increase of anisotropic viscosity [50]. The conceivable reason is that, the orderly molecular alignment forces the free volume to congregate along the orientation. The specific directional gathering of free volume leads to a sandwich-like microstructure, and the fracture and discontinuity are covered by staggered multi-layer chains. The void produced by free volume between two neighbor chains can absorb the shock from outside, and the strong intramolecular force prevents the dislocation developing along the fracture, which increase the energy dispassion and enhance the transverse toughness [57].

5. Conclusion

Based on the DMA and WAXD results, it is clear that the storage and loss modulus are associated with the molecular orientation for high-temperature stretched PC samples. The orientation of most of the low-temperature stretched specimens is higher than that of the high-temperature ones. The regular changes of dynamic viscoelasticity with orientation do not appear in the samples under the low-temperature condition. A relaxation equation deduced from the Elastic Dumbbell model has been successfully used in explaining the orientation
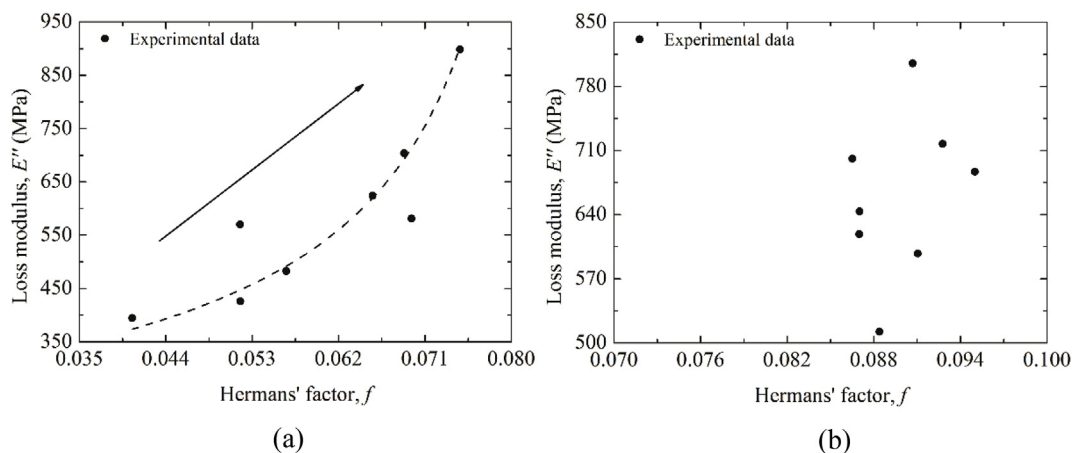
Fig. 7. The loss modulus versus average orientation of stretched specimens. ((a) and (b) represent the high-temperature and low temperature conditions, respectively.).

dependence of storage elasticity. The free volume theory and sandwich-like microstructure assumption were applied for interpreting the transverse loss modulus increase. The Deborah number is also introduced to interpret the increase of E' and E'' with increasing the orientation. The experimental results prove that the molecular theories can be used in the glass-like state of polymers. The dynamic dependence of viscoelasticity on molecular orientation during the deformation can be obtained analogically by the static images. DMA can be regarded as a new approach to determine the global orientation of high-temperature drawn PC sample. This research is helpful for understanding the mechanism of orientation and developing the new orientation characterization methods.

Acknowledgements

Appendix A. Supplementary data

Supplementary data related to this article can be found at http://dx.doi.org/10.1016/j.polymertesting.2018.06.009.

References

[1] M. Zaghdoudi, P.A. Albouy, Z. Tourki, A. Vieyres, P. Sotta, Relation between stress and segmental orientation during mechanical cycling of a natural rubber-based compound, J. Polym. Sci., Polym. Phys. Ed. 53 (2015) 943–950.
[2] F. Luo, X. Liu, C. Shao, J. Zhang, C. Shen, Z. Guo, Micromechanical analysis of molecular orientation in high-temperature creep of polycarbonate, Mater. Des. 144 (2018) 25–31.
[3] J. Jiang, X. Liu, M. Lian, Y. Pan, Q. Chen, H. Liu, G. Zheng, Z. Guo, D.W. Schubert, C. Shen, Self-reinforcing and toughening isotactic polypropylene via melt sequential injection molding, Polym. Test. 67 (2018) 183–189.
[4] Y. Pan, X. Liu, J. Kaschta, C. Liu, D.W. Schubert, Reversal phenomena of molten immiscible polymer blends during creep-recovery in shear, J. Rheol. 61 (2017) 759–767.
[5] X. Liu, Y. Pan, G. Zheng, H. Liu, Q. Chen, M. Dong, C. Liu, J. Zhang, N. Wang, E.K. Wujcik, T. Li, C. Shen, Z. Guo, Overview of the experimental trends in water-assisted injection molding, Macromol. Mater. Eng. 303 (2018) 1800035.
[6] X. Wang, Y. Pan, Y. Qin, M. Voigt, X. Liu, G. Zheng, Q. Chen, D.W. Schubert, C. Liu, C. Shen, , Creep and recovery behavior of injection-molded isotactic polypropylene with controllable skin-core structure, Polym. Test 69 (2018) 478–484.
[7] O. Hassager, Kinetic theory and rheology of bead-rod models for macromolecular solutions. II. Linear unsteady flow properties, J. Chem. Phys. 60 (1974) 4001–4008.
[8] O. Hassager, Kinetic theory and rheology of bead-rod models for macromolecular solutions. I. Equilibrium and steady flow properties, J. Chem. Phys. 60 (1974) 2111–2124.
[9] A.S. Lodge, Y.J. Wu, Constitutive equations for polymer solutions derived from the bead/spring model of Rouse and Zimm, Rheol. Acta 10 (1970) 539–553.
[10] J. Duhamel, A. Yekta, M.A. Winnik, T.C. Jao, M.K. Mishra, I.D. Rubin, A blob model

to study polymer chain dynamics in solution, J. Phys. Chem. 97 (1993) 13708–13712.
[11] P.G.D. Gennes, Reptation of a polymer chain in the presence of fixed obstacles, J. Chem. Phys. 55 (1971) 572–579.
[12] U. Ebert, Baumg, A. Auml, Sch, R. Auml, Short time behavior in de Gennes' reptation model, Phys. Rev. Lett. 78 (1997) 1592–1595.
[13] H.C. Ö, Modified reptation model, Phys. Rev. E 50 (1994) 4891–4895.
[14] P.D. Wu, E.V.D. Giessen, On improved network models for rubber elasticity and their applications to orientation hardening in glassy polymers, J. Mech. Phys. Solid. 41 (1993) 427–456.
[15] B.A. Beiermann, S.L.B. Kramer, P.A. May, J.S. Moore, S.R. White, N.R. Sottos, The effect of polymer chain alignment and relaxation on force-induced chemical reactions in an elastomer, Adv. Funct. Mater. 24 (2014) 1529–1537.
[16] M. Konda, H. Yamane, Y. Kimura, T. Kitao, Molecular mechanical analysis of polymer conformation, 2. Relation between chain conformation and birefringence of stretched non-crystalline polyurethanes with various substituent groups, Macromol. Chem. Phys. 195 (1994) 1985–2001.
[17] W.W.M. Jr., The measurement of molecular orientation in fibers by acoustic methods, J. Appl. Polym. Sci. 3 (1960) 266–276.
[18] Z. Li, R.J. Young, I.A. Kinloch, N.R. Wilson, A.J. Marsden, A.P.A. Raju, Quantitative determination of the spatial orientation of graphene by polarized Raman spectroscopy, Carbon 88 (2015) 215–224.
[19] M. Richardlacroix, C. Pellerin, Orientation and structure of single electrospun nanofibers of poly(ethylene terephthalate) by confocal Raman spectroscopy, Macromolecules 45 (2012) 1946–1953.
[20] M. Richard-Lacroix, C. Pellerin, Raman spectroscopy of individual poly(ethylene oxide) electrospun fibers: effect of the collector on molecular orientation, Vib. Spectrosc. 91 (2017) 92–98.
[21] D. Tao, Y. Higaki, W. Ma, H. Wu, T. Shinohara, T. Yano, A. Takahara, Chain orientation in poly(glycolic acid)/halloysite nanotube hybrid electrospun fibers, Polymer 60 (2015) 284–291.
[22] X. Liu, Y. Pan, C. Peng, X. Hao, G. Zheng, D.W. Schubert, C. Liu, C. Shen, Twisted lamellae in water-assisted injection molded high density polyethylene, Mater. Lett. 172 (2016) 19–22.
[23] X. Liu, G. Zheng, K. Dai, Z. Jia, S. Li, C. Liu, J. Chen, C. Shen, Q. Li, Morphological comparison of isotactic polypropylene molded by water-assisted and conventional injection molding, J. Mater. Sci. 46 (2011) 7830–7838.
[24] U. Stachewicz, S. Li, E. Bilotti, A.H. Barber, Dependence of surface free energy on molecular orientation in polymer films, Appl. Phys. Lett. 100 (2012) 3185–3217.
[25] C. Yan, J. Han, J. Zhang, F. Zhao, C. Liu, C. Shen, The influence of sub-T g annealing on environmental stress cracking resistance of polycarbonate, Polym. Test. 56 (2016) 364–368.
[26] C. Yan, J. Zhang, J. Han, X. Wang, Z. Guan, L. Zhang, C. Liu, C. Shen, Improvement of environmental stress cracking resistance of polycarbonate by silicone coating, Polym. Test. 60 (2017) 6–11.
[27] Q. Chen, J. Jing, H. Qi, I. Ahmed, H. Yang, X. Liu, T.L. Lu, A.R. Boccaccini, Electric field-assisted orientation of short phosphate glass fibers on stainless steel for biomedical applications, ACS Appl. Mater. Interfaces 10 (2018) 11529–11538.
[28] M. Qu, F. Nilsson, Y. Qin, G. Yang, Y. Pan, X. Liu, G.H. Rodriguez, J. Chen, C. Zhang, D.W. Schubert, Electrical conductivity and mechanical properties of melt-spun ternary composites comprising PMMA, carbon fibers and carbon black, Compos. Sci. Technol. 150 (2017) 24–31.
[29] Y. Pan, X. Liu, J. Kaschta, X. Hao, C. Liu, D.W. Schubert, Viscoelastic and electrical behavior of poly(methyl methacrylate)/carbon black composites prior to and after annealing, Polymer 113 (2017) 34–38.
[30] X. Hao, J. Kaschta, Y. Pan, X. Liu, D.W. Schubert, Intermolecular cooperativity and entanglement network in a miscible PLA/PMMA blend in the presence of nanosilica, Polymer 82 (2016) 57–65.
[31] X. Hao, J. Kaschta, X. Liu, Y. Pan, D.W. Schubert, Entanglement network formed in miscible PLA/PMMA blends and its role in rheological and thermo-mechanical

properties of the blends, Polymer 80 (2015) 38–45.

[32] Y. Pan, D.W. Schubert, J.E. Ryu, E. Wujick, C. Liu, C. Shen, X. Liu, Dynamic oscillatory rheological properties of polystyrene/poly(methyl methacrylate) blends and their composites in the presence of carbon black, Eng. Sci. 1 (2018) 86–94.

[33] N.T. Qazvini, N. Mohammadi, Dynamic mechanical analysis of segmental relaxation in unsaturated polyester resin networks: effect of styrene content, Polymer 46 (2005) 9088–9096.

[34] R. Pantani, A. Sorrentino, V. Speranza, G. Titomanlio, Molecular orientation in injection molding: experiments and analysis, Rheol. Acta 43 (2003) 109–118.

[35] A.K. Kalkar, H.W. Siesler, F. Pfeifer, S.A. Wadekar, Molecular orientation and relaxation in poly(butylene terephthalate)/polycarbonate blends, Polymer 44 (2003) 7251–7264.

[36] H. Schiessel, R. Metzler, A. Blumen, T.F. Nonnenmacher, Generalized viscoelastic models: their fractional equations with solutions, J. Phys. Math. Gen. 28 (1999) 6567.

[37] K.S. Fancey, A mechanical model for creep, recovery and stress relaxation in polymeric materials, J. Mater. Sci. 40 (2005) 4827–4831.

[38] Y. Pan, X. Guo, G. Zheng, C. Liu, Q. Chen, C. Shen, X. Liu, Shear-Induced Skin-Core Structure of Molten Isotactic Polypropylene and the Formation of β-Crystal, Macromol. Mater. Eng. 303 (2018) 1800083.

[39] K. Kroy, E. Frey, Force-extension relation and plateau modulus for wormlike chains, Phys. Rev. Lett. 77 (1996) 306.

[40] O. Kratky, G. Porod, Diffuse small-angle scattering of X-rays in colloid systems, J. Colloid Sci. 4 (1949) 35–70.

[41] F. Gittes, F.C. Mackintosh, Dynamic shear modulus of a semiflexible polymer network, Phys. Rev. E 58 (1998) R1241–R1244.

[42] C.P. Broedersz, F.C. MacKintosh, Modeling semiflexible polymer networks, Rev. Mod. Phys. 86 (2016) 995–1036.

[43] D.J. Blundell, A. Mahendrasingam, D. Mckerron, A. Turner, R. Rule, R.J. Oldman, W. Fuller, Orientation changes during the cold drawing and subsequent annealing of PEEK, Polymer 35 (1994) 3875–3882.

[44] J.S. Vrentas, C.M. Jarzebski, J.L. Duda, A Deborah number for diffusion in polymer-solvent systems, AIChE J. 21 (1975) 894–901.

[45] S.J. Picken, J. Aerts, R. Visser, M.G. Northolt, Structure and rheology of aramid solutions: x-ray scattering measurements, Macromolecules 23 (1990) 3849–3854.

[46] X. Liu, K. Dai, X. Hao, G. Zheng, C. Liu, D.W. Schubert, C. Shen, Crystalline structure of injection molded β-isotactic polypropylene: analysis of the oriented shear zone, Ind. Eng. Chem. Res. 52 (2013) 11996–12002.

[47] Y. Pan, X. Liu, S. Shi, C. Liu, K. Dai, R. Yin, D.W. Schubert, G. Zheng, C. Shen, Annealing induced mechanical reinforcement of injection molded iPP parts, Macromol. Mater. Eng. 301 (2016) 1468–1472.

[48] Z. Liu, X. Liu, G. Zheng, K. Dai, C. Liu, C. Shen, R. Yin, Z. Guo, Mechanical enhancement of melt-stretched β-nucleated isotactic polypropylene: the role of lamellar branching of β-crystal, Polym. Test. 58 (2017) 227–235.

[49] X. Liu, M. Lian, Y. Pan, X. Wang, G. Zheng, C. Liu, D.W. Schubert, C. Shen, An alternating skin-core structure in melt multi-injection-molded polyethylene, Macromol. Mater. Eng. 303 (2018) 1700465.

[50] Y. Zhuang, S. Ando, Evaluation of free volume and anisotropic chain orientation of Tröger's base (TB)-based microporous polyimide/copolyimide membranes, Polymer 123 (2017) 39–48.

[51] Y. Song, K. Nitta, N. Nemoto, Deformation mechanisms of polymer thin films by simultaneous kinetic measurement of microscopic infrared dichroism and macroscopic stress. 2. Molecular orientation during necking process of isotactic polypropylene, Macromolecules 36 (2003) 132–138.

[52] R.Z. Lu, Y. Pan, X. Liu, G. Zheng, D.W. Schubert, C. Liu, Molar mass and temperature dependence of rheological properties of polymethylmethacrylate melt, Mater. Lett. 221 (2018) 62–65.

[53] C.B. Bucknall, R.R. Smith, Stress-whitening in high-impact polystyrenes, Polymer 6 (1965) 437–446.

[54] T. Odijk, The statistics and dynamics of confined or entangled stiff polymers, Macromolecules 16 (1983) 1340–1344.

[55] M.D. Shelby, G.L. Wilkes, The effect of molecular orientation on the physical ageing of amorphous polymers—dilatometric and mechanical creep behaviour, Polymer 39 (1998) 6767–6779.

[56] P.I. Vincent, The necking and cold-drawing of rigid plastics, Polymer 1 (1960) 7–19.

[57] I. Greenfeld, X.M. Sui, H.D. Wagner, Stiffness, strength, and toughness of electrospun nanofibers: effect of flow-induced molecular orientation, Macromolecules 49 (2016) 6518–6530.